# 6 Influence of curvature and aspects linked to the one dimensional semi-infinite hypothesis

## 6.1 Introduction

According to the analysis in chapter 5, the comparison of the measurements in the CT3 facility between the two-layer gauges and the single-layer ones at 50% of the second stator blade was successful for all the gauges except the ones at the stagnation region (511 and 211). Moreover, although the stagnation region is highly curved compared to the rest of blade profile, the wall heat flux calculations at the stagnation are also based on the semi-infinite flat plate geometry (chapter 3). It could be hence claimed that the difference between the two stagnation gauges has its origin in the curvature effects that are not taken into account during the wall heat flux calculations. Apparently, two dimensional calculations could diminish the 50% difference between the two techniques and/or clarify the reasons of this difference in one dimensional calculations. However, the two dimensional analysis uses as a boundary condition the wall temperature around the blade profile, which was not measured. Thus, the following paragraphs are an attempt to quantify the above 50% difference by simpler taking into account the curvature influence on the one dimensional calculations.

## 6.2 Influence of the curvature on the Nusselt number calculations

### *6.2.1 Introduction to curvature influence*

Till now all the calculations of the heat transfer data were performed assuming a flat geometry, so possible errors are introduced when the surface is actually curved. The magnitude of such errors will depend on how far the heat penetrates into the substrate in comparison to the radius of curvature of the surface (Buttsworth and Jones, 1997). There is an approximate solution which indicates that it is relatively straight forward to correct heat flux data obtained on the basis of a semi-infinite flat plate analysis $Q_{W,FP}$, providing that the heat penetrates only a relatively small distance into the substrate such that $\alpha t / R^2 << 1$:

$$Q_W = Q_{W,FP} - \frac{k\sigma}{2R}\left(T_W - T_{INIT}\right) , \tag{37}$$

where $\alpha$ stands for the thermal diffusivity of the substrate, $t$ for the time during which $Q_W$ is applied, $R$ for the radius of curvature of the substrate, $k$ for the thermal conductivity of the substrate, $T_{INIT}$ for the substrate temperature prior to the application of the $Q_W$; $\sigma$ is equal to $1$ for a cylindrical substrate and to $2$ for a spherical substrate. (Note that in the following chapter $Q_W$ is considered to be the actual wall heat flux, while the one calculated with the analysis described in chapters 3, 4 and 5 (semi-infinite flat plate) is represented by the new notation $Q_{W,FP}$ .) Equation (37) can be used to estimate the minimum radius $R_{MIN}$ of a cylindrical geometry ($\sigma = 1$) that corresponds to a correction of less than *10%* on the heat flux calculations for single-layer gauges on a Macor substrate ($k = 1.851\ W/mK$). During the tests in the CT3 facility with the single-layer gauges (chapter 4), the temperature difference ($T_W - T_{INIT}$) is of the order of $16.5\ K$ at the leading edge and the corresponding heat flux calculated from the flat plate geometry ($Q_{W,FL}$) is around $70\ kW/m^2$ (gauge 211). Then the calculations require a minimum radius of *2.2 mm*. Note that this value is even higher than the radius of the blade profile at the position of the gauge 211. In Table 6-1, the radii of curvature of the blade for the three positions, which are located around the stagnation region, are indicated. They are calculated by using the cross section of the blade as well as the local first ($x'$) and second ($x''$) derivatives:

$$R = \frac{\sqrt{\left(1 + x'^2\right)^3}}{x''} \ . \tag{38}$$

| Gauge | Position ($S / S_{MAX}$) | Radius (mm) |
|---|---|---|
| 211 or 511 | -0.00349 | 1.749 |
| 210 | -0.02275 | 3.337 |
| 212 | 0.015944 | 3.410 |

**Table 6-1: Radius of the blade at the three positions in the stagnation region**

Moreover, Eq. (37) indicates that for the same wall heat flux $Q_W$, the wall temperature rise for a cylinder $\Delta T_{W,CYL}$ is higher than for a plate $\Delta T_{W,FP}$ of the same material, of the same value of $k$ and of length $L$ equal to the diameter of the cylinder $2R$ (see Figure 6-1). The higher wall temperature on the cylinder is because of its smaller volume to area ratio exposed to the heat flux in comparison to the flat plate, which means that it has lower thermal inertia (mass, $m$, times specific heat, $c$). The following equation gives a quantitative overview of the above concept:

$$Q = m \ c \ \Delta T_W \ . \tag{39}$$

Summarizing the above conclusions, it is evident that the wall heat flux, which is calculated with the flat plate geometry (chapters 4 and 5) close to the stagnation region (gauge 211 and 511, 210, 212), where the curvature effects are significant, is higher than its real value. Before the curvature effects are discussed around the stagnation region, some information is given about the heat flux calculations based on flat geometry or on a cylindrical one, and about their limitations in comparison to real heat transfer phenomenon.

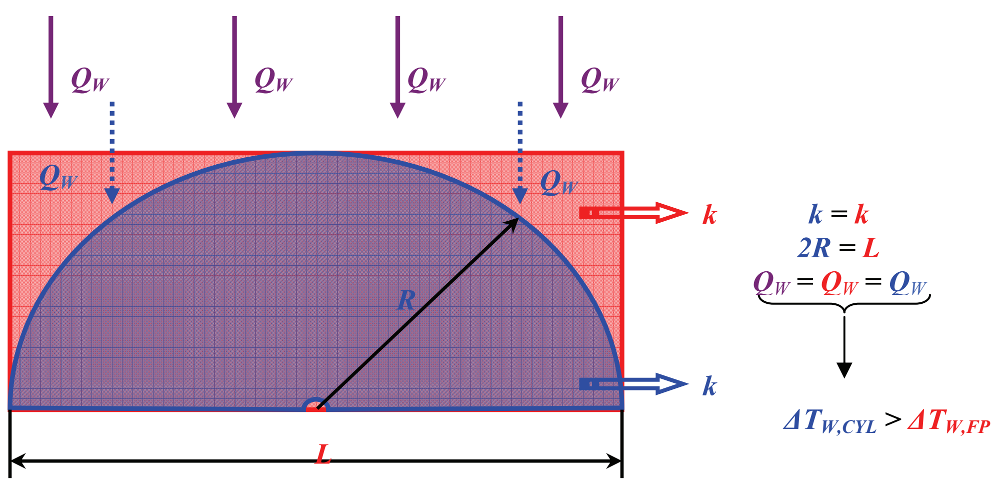


**Figure 6-1: Convection on a flat plate and a cylinder**

### 6.2.2 *Convection on the stagnation region of the blade*

The stagnation region of the blade is curved in such a way that the convection around a cylinder can be used as an approximation. This region of the blade can be locally represented by a cylinder whose radius is equal to the radius of curvature of the blade contour (the representative values at the position of the gauges are given in Table 6-1 and shown graphically in Figure 6-2). A data reduction program that calculates the wall heat flux in the stagnation region with a cylindrical geometry that takes into account the curvature instead of a flat plate is a better approximation.

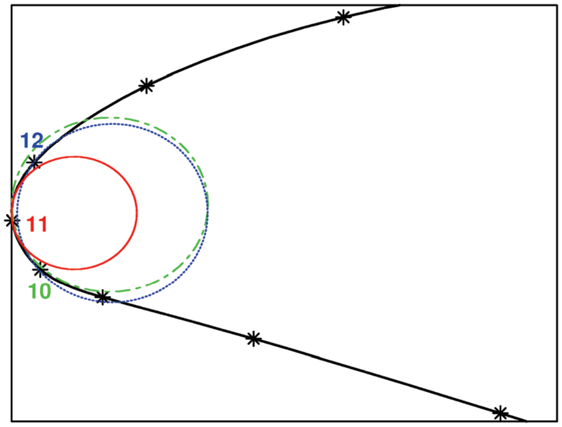


**Figure 6-2: Graphical representation of the radius of the blade at the three positions in the stagnation region**

### *6.2.3 Limitations of the cylindrical geometry in the data reduction program*

The one dimensional conduction equation in cylindrical coordinates applied on a curved single-layer gauge (Eq. (40)) is solved in the data reduction program instead of Eq. (3), in order to take into account the curvature effects:

$$\frac{\partial}{\partial r}\left[k(T)\frac{\partial T}{\partial r}\right]+k(T)\frac{\sigma}{r}\frac{\partial T}{\partial r}=\rho c(T)\frac{\partial T}{\partial t}\ , \tag{40}$$

where *k, ρ, c* stand for the thermal conductivity, the density and the specific heat of the substrate, $\sigma$ is equal to 1 and $T$ is a function of radial coordonate and time ($T(r,t)$). The first boundary condition in Eq. (40) is the symmetry applied at the center of the substrate (Eq. (41), $r=R$) and it does not impose the semi-infinite condition. Thus, a final check is necessary to validate the semi-infinite concept on the wall heat flux calculation (Eq. (42)). The second boundary condition is the wall temperature history measured during the test; the initial temperature in the gauge substrate is uniform and known:

$$\left(\frac{\partial T}{\partial r}\right)_{r=R,t}=0\ , \tag{41}$$

$$Q_W=-k\left(\frac{\partial T}{\partial r}\right)_{r=0,t}\ . \tag{42}$$

More about Eq. (40) is given in paragraphs 10.3, 10.4 and 10.5.

The calculations of the heat flux with the curvature correction approximate the real case of the blade convection, when the integration time is short, or the radius of the blade is large in such a way that the condition $\alpha t\,/R^2 <<1$ is valid (paragraph 6.2.1). Then the semi-infinite condition at the center of the cylindrical geometry is also verified.

### *6.2.4 Curvature correction on Nusselt number calculations*

The three gauges that are considered to suffer the most from curvature effects are the ones around the stagnation region, 210, 211, 212. For these three gauges the wall heat flux is calculated twice, once with the flat plate geometry (chapter 4) and once with the cylindrical geometry, using the diameter given in Table 6-1. A difference of about *15%* on the wall heat flux between the two approaches is observed for the gauge 211. The difference is lower for the other two gauges, because the curvature is smaller. In Figure 6-3, the average Nusselt number distribution, calculated from the flat geometry approximation is shown for the single-layer and two-layer gauges (circles). On the same graphs, the Nusselt number calculated from cylindrical geometry is compared (diamonds) for gauges 210, 211, 212 and 511 respectively.

More specifically, as far as the single-layer gauges are concerned, the correction of the Nusselt number due to the curvature on gauge 211 is *(4000-3600) / 4000 *100% = -15%*, which is not negligible. Unfortunately, for the two-layer gauges, there is only one gauge in this region of the blade and the equivalent gauges 509, 510, 512, 513 were not implemented. Thus, as far as the gauge 511 is concerned, it seems that the curvature correction of the Nusselt number calculations is much smaller than the one of its equivalent single-layer gauge, around *(5900-5500) / 5900 *100% = -6.7%.*

The correction of the Nusselt number due to curvature effects increases even more the difference on the Nusselt number calculations between the single-layer and the two-layer gauges at the stagnation point of the blade, a difference that is already high from the flat geometry calculations. Therefore, the curvature effects at this region are not the real source of the above Nusselt number difference.

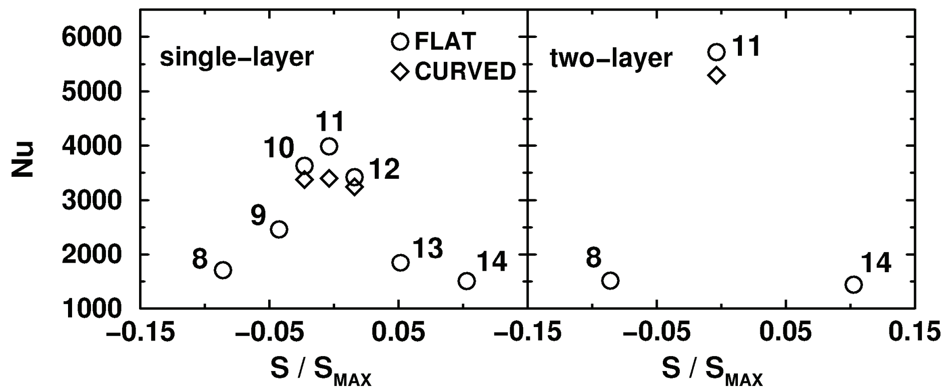


**Figure 6-3: Curvature correction for gauges 210, 211, 212, 511**

| Turbulence | Smith and Kuethe | Kestin and Wood | Lowery and Vachon |
|---|---|---|---|
| 0.02 | 3823 | 3668 | 3847 |
| 0.05 | 4112 | 4002 | 4100 |
| 0.10 | 4593 | 4507 | 4482 |

**Table 6-2: Nusselt number calculations at the position 11 of the blade based on three different empirical correlations referred to cylinders in cross-flow**

The Nusselt number at the stagnation point of the blade (position of the gauges 511 and 211) is also calculated based on three different empirical correlations used for cylinders in cross-flow (Table 6-2). Although these three empirical correlations (Smith and Kuethe (1966), Kestin and Wood (1971) and Lowery and Vachon (1975)) are from three different references, the Nusselt number calculations are very close to each other. Note that the latter depends on the turbulence intensity of the flow. However, even extreme values of turbulence intensity could not eventually explain the high values of *5900* for the Nusselt number calculations performed on the two-layer gauge.

## 6.3 Semi – infinite condition for the curvature correction approach

In Figure 6-4, the temperature and the heat flux history (calculated from the cylindrical geometry data reduction program) of the single-layer gauge at the stagnation point of the blade (gauge 211) from a representative test are shown at three different radial positions. More precisely, it is the temperature change of the gauge at the surface, at the center and at a distance of *175 μm* from the surface of the blade. (Note that this distance corresponds to the calibrated thickness of the Upilex layer and the glue for the equivalent case of the two-layer gauges.) The two vertical blue lines on the same graph indicate the time limits that are used for the time - averaged component of the Nusselt number calculations. As one can easily notice, the temperature at the center remains equal to the initial one during the entire data reduction time and then it starts slightly rising. Thus, the semi-infinite condition at the center of the cylindrical geometry is still valid for the Nusselt number calculations with curvature as far as the single-layer gauges are concerned.

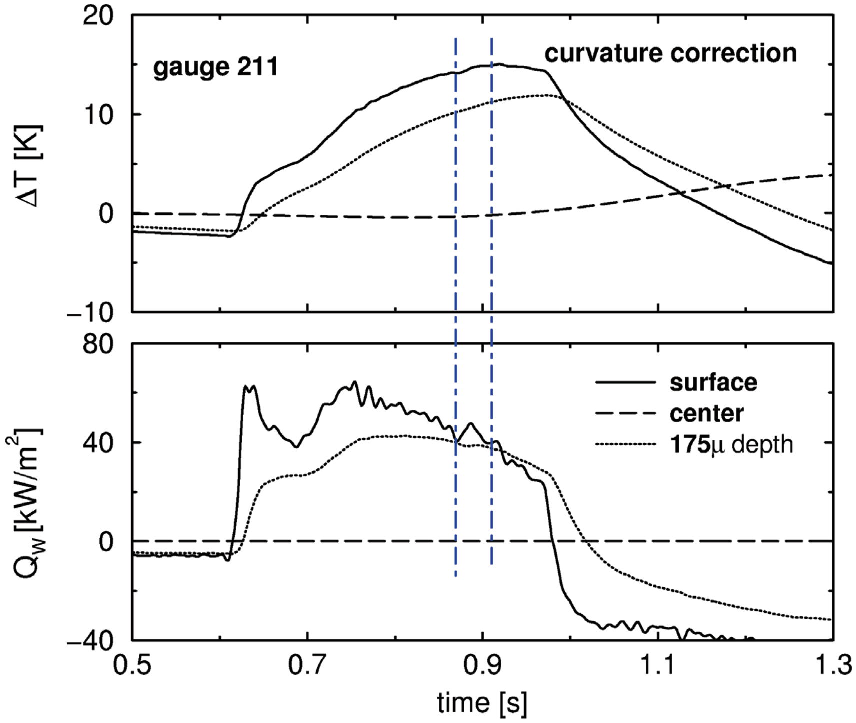


**Figure 6-4: Temperature and heat flux history for the gauge 211 in three different radial positions**

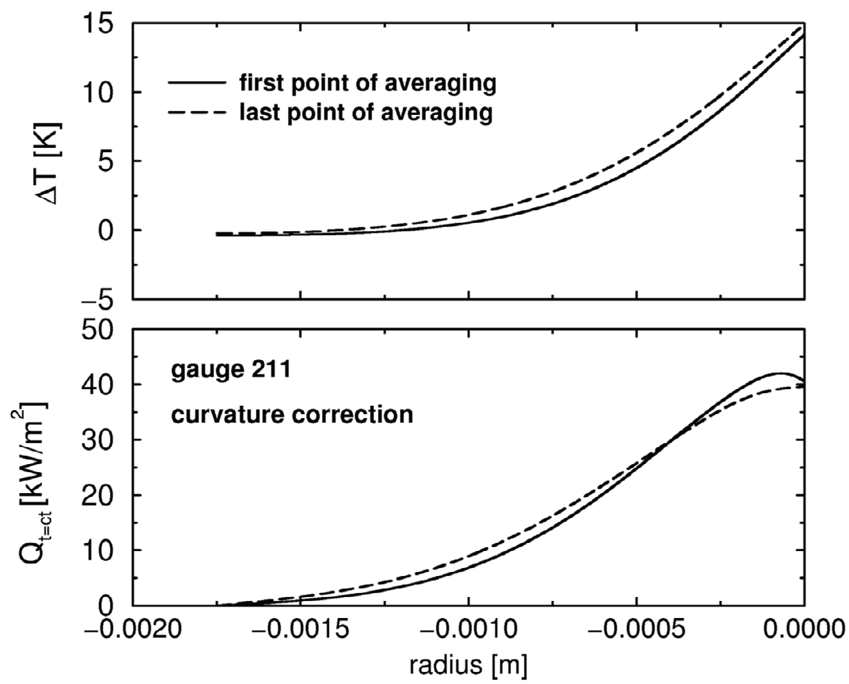


**Figure 6-5: Temperature and heat flux distribution of gauge 211 as a function of the radial position at two different calculation times**

The same conclusion is illustrated in Figure 6-5, where the temperature variation and the heat flux distribution across the total radius of the cylindrical approximation of the substrate are shown for two different time steps: the beginning (first point of averaging) and the end (last point of averaging) of the time interval used for the calculation of the time–averaged component of the Nusselt number (the two blue vertical lines in Figure 6-4). For both time cases the temperature at the center is equal to the initial one ($\Delta T = T(_{r=R=1.749mm}) - T_{INIT} = 0$).

As far as the gauges 210 and 212 are concerned, the same analysis can be performed on them and the same conclusions can be drawn, with the advantage that the radial effects will be even lower, as the radii are higher. Note that the data reduction time interval for the Nusselt number calculations is the same for all the single-layer gauges.

The same analysis is carried out for the gauge 511 of the two-layer series. Equation (40) is applied for the two substrates; the temperature and heat flux at the interface of the two substrates are set equal. In Figure 6-6, the temperature variation and the heat flux history with curvature effects are shown at the surface, at the center and at a depth of *175 μm* from the surface of the blade (Upilex with glue thickness). In this case, the temperature at the center is not equal to its initial value across the time interval of the time - averaged component of the Nusselt number calculations (time between the two blue vertical lines). Thus, the semi-infinite condition at the center of the cylindrical geometry is not valid for the Nusselt number calculations as far as the two- layer gauge is concerned.

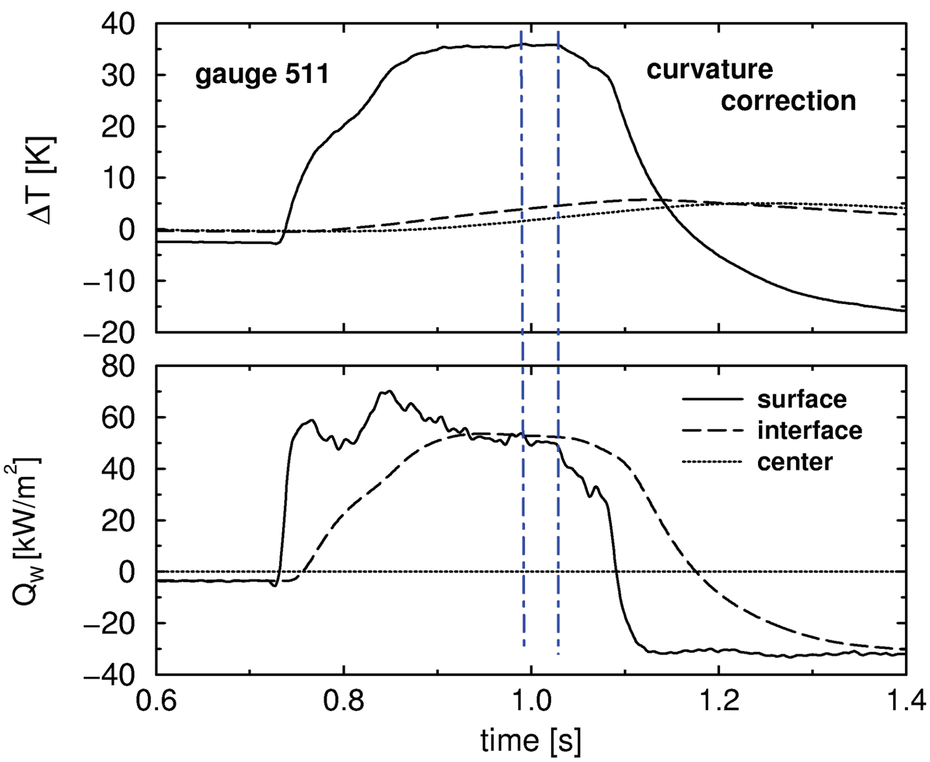


**Figure 6-6: Temperature and heat flux history for the gauge 511 in three different radial positions**

The latter can also be verified from Figure 6-7, where the temperature variation and the heat flux distribution of gauge 511 across the radius are shown for the beginning and the end of the time limits used for the Nusselt number calculation. The temperature at the center for each time step rises by *1.5* and *2.2 K* respectively.

As the semi-infinite condition is not valid any more, it is possible that additional mistakes are introduced on the above calculations. If the cylinder that approximates the gauge geometry for the above Nusselt number calculations is split into two parts (half cylinder, which simulates the stagnation region of the blade exposed to the flow and half cylinder behind the flow), then the symmetry condition implies that whatever happens in the half front part of the cylinder should also happen at the other half part of the cylinder. At the limit that the temperature at the center is not zero, then problems arise during the wall heat flux calculations.

Summarizing Figure 6-6 and Figure 6-7, it seems that the application of Eq. (40) in two layers should be used with precaution and introduces the need of a two dimensional (2D) calculation inside the substrate, where the correct geometry of the blade profile can be used without the requirement of the semi-infinite condition. Note that the 2D analysis will also take into account the lateral conduction effects inside the blade that are considered negligible in this work.

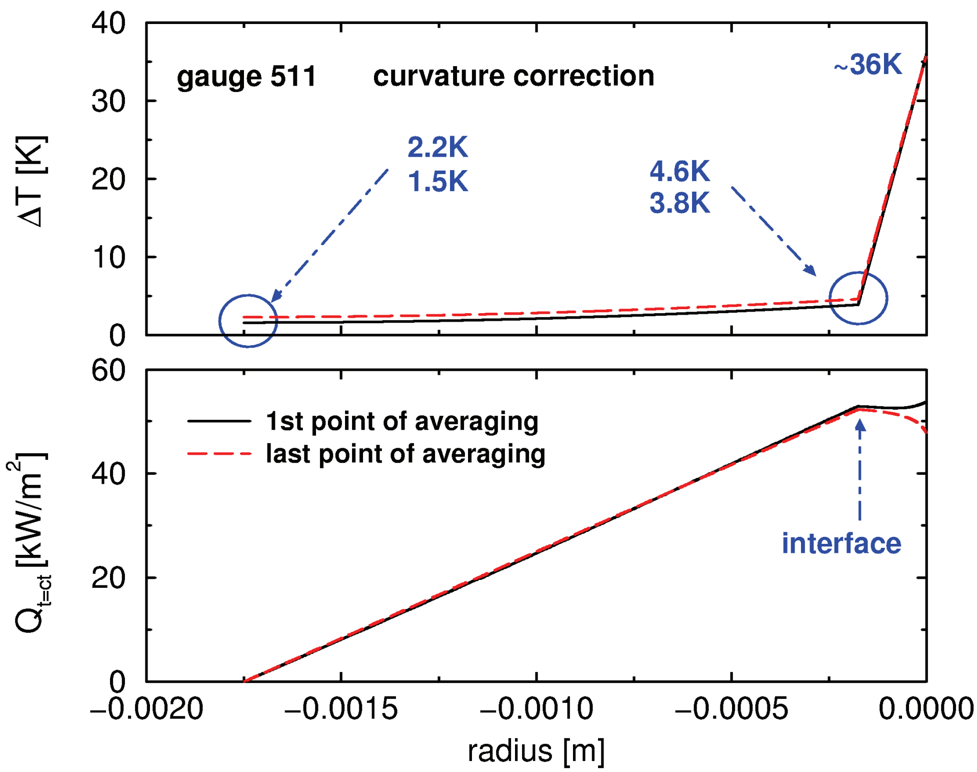


**Figure 6-7: Temperature and heat flux distribution of gauge 511 as a function of the radial position for two different times**

## 6.4 Additional comments on the Nusselt number calculations

### *6.4.1 A qualitative attempt to explain the influence of the metallic substrate on the heat flux calculations*

If there is a uniform wall heat flux applied on the blade (see Figure 6-8), then the gauge measures a corresponding wall temperature variation (shown in red). In case that lateral conduction exists (shown in blue), for the same wall heat flux vertical to the gauge substrate, the wall temperature is lower than the one for the case where the lateral conduction is negligible. If the same data reduction program is used, based on the one dimensional heat conduction, then a heat flux (calculation with lateral conduction) lower than the real one (reality) is calculated. During the test in CT3 facility, the gauge measures the correct wall temperature increase; if there was 2D conduction, the calculated wall heat flux with the one dimensional approach is much lower than the 2D one. In other words, if the lateral conduction effect is taken into account for the time-averaged Nusselt number calculations of the two-layer gauge, then the new values will be even higher than the one dimensional approach (in case that the lateral conduction is not negligible). The same conclusion can be applied for the single-layer gauge. However, as the second layer of the two-layer gauge is made of metal, the lateral conduction is expected to be faster and stronger on the two-layer gauge than the single-layer gauge and thus the difference between the single and two-layer gauges will increase even more at the stagnation point of the blade.

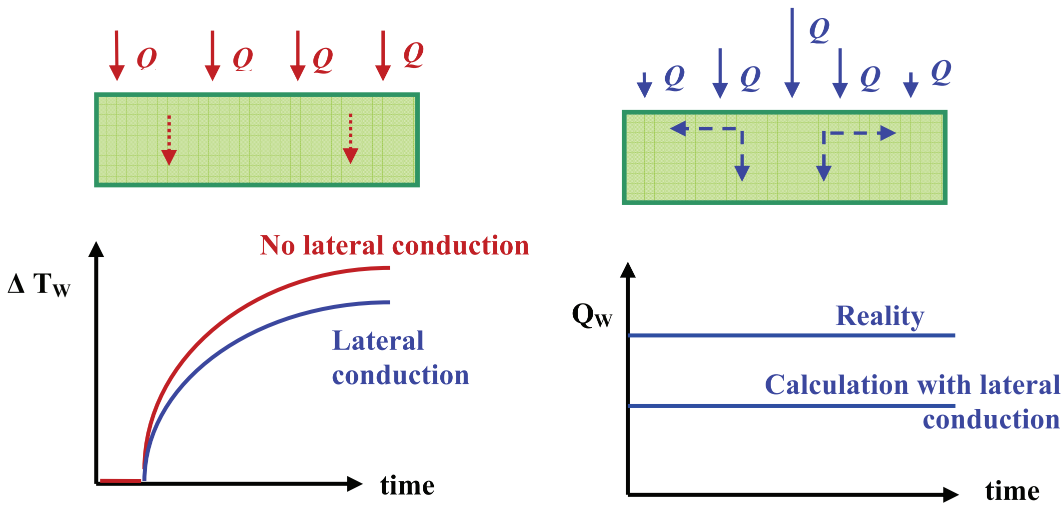


**Figure 6-8: Lateral conduction effects on the wall heat flux calculations**

It would be practical if the thickness of the Upilex could be increased, so that the semi-infinite condition is reached with one layer already for both cases with and without curvature correction. Then, the procedure for the heat flux calculations would be closer to the one of the single-layer gauges, which is well certified. On the other hand, the thickness of Upilex has to be still small enough to be able to be glued on any kind of blade geometry.

As far as the whole analysis of this chapter for the two-layer gauges is concerned, the solution of the heat conduction in the metallic substrate with a 2D approach could explain better the Nusselt number distribution on the blades. This requires much more effort, as firstly one has to define the grid inside the blade profile and then to solve the heat conduction equation in two dimensions, using two coordinates (x,y) and two second order spatial derivatives of temperature for two different materials (different thermal properties).

This work requires:

*a)* special knowledge on grid generation (because of the high complexity of the blade profile),
*b)* special care on the discretization of the 2D conduction equation,
*c)* accurate application of the boundary conditions (the amount of the heat flux that leaves the first layer should be equal to the wall heat flux minous the one used for heating up the first layer),
*d)* a physical conception of the distribution of the wall temperature around the whole blade profile from the discrete measurements.

All these requirements should be combined in one program capable to calculate the wall heat flux distribution vertical to the blade profile from the wall temperature measurements. The complexity of the above mentioned work together with the necessity to better control the Nusselt number distribution around the blade profile could finally suggest the 2D approach as the subject of another independent work in the future.

### *6.4.2 Note on the adiabatic wall temperature for the Nusselt number definition*

In all the analysis described in chapters 4 and 5, the Nusselt number Eq. (30) is defined based on the total gas temperature, $T_{GAS}$. A substitution of temperature $T_{GAS}$ with the adiabatic wall temperature, $T_{AW}$, does not significantly change the Nusselt number values for the tests in the CT3 facility, at the blade leading edge. The reason is:
*a)* because $T_{GAS}$ is equal to $T_{AW}$ at the stagnation point (appendix 18.5),
*b)* because the tests are performed with low velocity fluid (the inlet absolute Mach number is *0.43*) and thus the effects of viscous dissipation are considered negligible.
More information about the definition of the Nusselt number was given by Kays and Crawford (1980).

In addition, the adiabatic wall temperature around the blade profile can not be determined experimentally, while the gas temperature can be measured by a thermocouple in an easy, fast and repeatable way.

## 6.5 References

Buttsworth D.R., Jones T.V., 1997, *'Radial conduction effects in transient heat transfer experiments',* The Aeronautical Journal, Vol. May, p.p. 209-212

Smith M. and Kuethe A., 1966, *'Effects of turbulence on laminar skin friction and heat transfer',* Physics of fluids, vol. 9, pp 2337-2344

Kestin J., Wood R., 1971, *'The influence of turbulence on mass transfer from cylinders',* J. of Heat Transfer, vol. 93(C), pp 321-327

Lowery G. W. and Vachon R.I., 1975, *'The effect of turbulence on heat transfer from heated cylinders',* Int. J. of Heat and Mass Transfer, vol. 18, pp 1229-1242